Received: 24 November 2020 | Revised: 27 August 2021 | Accepted: 31 August 2021

DOI: 10.1002/hyp.14368

SCIENTIFIC BRIEFING

HP TODAY WILEY

Estimation of sub-annual inter-catchment groundwater flow using short-term water balance method

Tomohiro Egusa[1,2] | Tomoki Oda[1,3] | Takanori Sato[4] | Tomo'omi Kumagai[1,5,6]

[1]Graduate School of Agricultural and Life Sciences, The University of Tokyo, Tokyo, Japan

[2]Faculty of Agriculture, Shizuoka University, Shizuoka, Japan

[3]Forestry and Forest Products Research Institute, Tsukuba, Japan

[4]Ecohydrology Research Institute, The University of Tokyo Forests, Graduate School of Agricultural and life Science, The University of Tokyo, Seto, Japan

[5]Institute for Space-Earth Environmental Research, Nagoya University, Nagoya, Japan

[6]Water Resources Research Center, University of Hawai'i at Mānoa, Honolulu, Hawaii, USA

Correspondence
Tomohiro Egusa, Graduate School of Agricultural and Life Sciences, The University of Tokyo, 1-1-1 Yayoi, Bunkyo-ku, Tokyo 113-8657, Japan.
Email: tomohiroegusa@gmail.com

Abstract

Predicting inter-catchment groundwater flow (IGF) is essential because IGF greatly affects stream water discharge and water chemistry. However, methods for estimating sub-annual IGF and clarifying its mechanisms using minimal data are limited. Thus, we quantified the sub-annual IGF and elucidated its driving factors using the short-term water balance method (STWB) for three forest headwater catchments in Japan (named here catchment A, B and As). Our previous study using the chloride mass balance indicated that annual IGF of catchment A (49.0 ha) can be negligible. Therefore, we calculated the daily evapotranspiration (ET) rate using the Priestley–Taylor expression and the 5-year water balance in catchment A (2010–2014). The sub-annual IGF of the three catchments was then calculated by subtracting the ET rate from the difference between rainfall and stream discharge during the sub-annual water balance periods selected using the STWB. The IGF rates of catchment B (7.0 ha), which is adjacent to catchment A, were positive in most cases, indicating that more groundwater flowed out of the catchment than into it, and exhibited positive linear relationships with rainfall and stream discharge. This suggested that as the catchments became wetter, more groundwater flowed out of catchment B. Conversely, the IGF rates of catchment As (5.3 ha), included in catchment A, were negative in most cases, indicating that more groundwater flowed into the catchment than out from it, and exhibited negative linear relationships with rainfall and stream discharge. Given the topography of the catchments studied, infiltration into the bedrock was the probable reason for the IGF outflow from catchment B. We hypothesized that in catchment As, the discrepancy between the actual hydrological boundary and the surface topographic boundary could have caused an IGF inflow. This study provides a useful tool for determining an IGF model structure to be incorporated into rainfall-runoff models.

KEYWORDS
bedrock infiltration, catchment water balance, evapotranspiration, rainfall-runoff modelling, stream discharge, water imbalance

1 | INTRODUCTION

Inter-catchment groundwater flow (IGF) represents the gains and losses of groundwater that cross catchment boundaries (Eakin, 1966). Previous studies have demonstrated that the IGF rate can be as high as a few tens of percent of rainfall and could not be negligible in catchments with a wide range of geologies (such as sandstone, granodiorite, andesite and lava) and climates (e.g., arid, temperate, tropical;

Aishlin & McNamara, 2011; Genereux et al., 2005; Graham et al., 2010; Manna et al., 2016; Oda et al., 2013). IGF recharges groundwater storage in mountain blocks (Manning & Solomon, 2005; Thoma et al., 2011) and discharges more with increasing catchment area (Egusa et al., 2016; Frisbee et al., 2011). Such groundwater generally has a long residence time, and its dissolved matter concentrations are greatly influenced by geochemical evolution (Frisbee et al., 2016; Genereux et al., 2009). Therefore, IGF largely affects not only stream water discharge, but also dissolved matter concentrations and the subsequent chemical balance of small to large catchments (Egusa et al., 2016; Genereux et al., 2005; Peralta-Tapia et al., 2015).

Because IGF is fundamentally the movement of water due to the hydraulic gradient, including the effects of pressure propagation, its rate is likely to change dynamically according to temporal changes in water storage inside the catchments (Kormos et al., 2015; Kosugi et al., 2006). Temporal changes in water storage are almost negligible on long time scales such as annual; however, they become apparent on sub-annual time scales. Therefore, to detect changes in IGF in accordance with changes in water storage and elucidate IGF mechanisms, it is necessary to derive IGF in sub-annual time steps. Among existing methods, the catchment water balance (Flerchinger & Cooley, 2000; Katsuyama et al., 2010; Schaller & Fan, 2009) and the catchment mass balance of ions (Aishlin & McNamara, 2011; Genereux et al., 2005; Manna et al., 2016; Oda et al., 2013) are typically applied to obtain IGF on a yearly time scale. When more detailed time steps were selected using these methods, additional data, such as soil water content (Graham et al., 2010; Kormos et al., 2015), or additional assumptions, such that the difference between recession curves of stream discharge and power law curves represented the rate of IGF (Wang, 2011) were needed. The estimation method based on Darcy's law with multipoint groundwater level data (Thyne et al., 1999) allowed us to analyse the IGF mechanism at the same time step as the observation. However, this method requires significant costs for multipoint observations of groundwater and is largely influenced by the spatial heterogeneity of groundwater levels and transmissivity. The most common method for estimating IGF at sub-annual time steps is to incorporate the IGF sub-models into rainfall-runoff models and determine their parameters with parameter fitting procedures (Bouaziz et al., 2018; Le Moine et al., 2007; Manna et al., 2019; Voeckler et al., 2014; Zanon et al., 2014).

However, IGF estimation using rainfall-runoff models is not an ideal method and has certain limitations. Application of rainfall-runoff models has indicated that the difference in model structure had a significant influence on stream discharge calculation results (Clark et al., 2008; Fenicia et al., 2008; McMillan et al., 2011). It is no exception for IGF, and how to incorporate IGF sub-models into rainfall-runoff models is an important issue. Some studies on IGF have attempted to decide the structure of IGF sub-models by comparing observed stream discharge and the calculation results of rainfall-runoff models that incorporate different IGF sub-models (Bouaziz et al., 2018; Le Moine et al., 2007). In such IGF structure comparisons, when model structures are complex and/or the number of model structures and parameters to be compared are large, parameter fitting becomes increasingly difficult. In addition, such comparisons are expected to suffer from the problem of equi-finality such that a specific model structure and a parameter set could not be identified because of equally good fit of models with different parameters and model structures (Beven, 1993). Therefore, we require a method for estimating sub-annual IGF that does not use rainfall-runoff models and ensures IGF estimation on a time scale enabling extraction of changes in dry/wet conditions of catchments from limited data such as rainfall and stream discharge. Such a method would not only be useful for estimating IGF but also would serve as a tool to investigate processes driving IGF and to determine IGF model structure.

This study focused on the short-term water balance method (STWB; Linsley et al., 1958). The STWB assumes that when the difference in stream discharges between certain moments in time is small, the difference in water storage between those moments in time is also small. Due to this assumption, we can ignore the temporal changes in water storage in the sub-annual water balances. The STWB has been generally used to estimate seasonal changes in evapotranspiration (ET) assuming little IGF (Kondo et al., 1992; Kosugi & Katsuyama, 2007; Suzuki, 1985). We used the STWB for estimating sub-annual IGF by calculating ET with the Priestley and Taylor equation (Priestley & Taylor, 1972) and the annual water balance.

Our objectives were to quantify sub-annual IGF and investigate physical processes driving IGF for IGF modelling in three headwater catchments, Japan. First, we parameterized an ET model using the 5-year water balance of a catchment where annual IGF was negligible. Then, the sub-annual IGF at each studied catchment was estimated as the residual of its water balance applied by the modelled ET. Finally, we examined the relationships between the estimated sub-annual IGF and hydrological factors.

2 | MATERIALS AND METHODS

2.1 | Study site

We studied three forest headwater catchments (catchment A, catchment B and catchment As) in the Oborasawa Experimental Watershed (OEW), located in the Tanzawa Mountains in Japan (35°28′N, 139°12′E; Figure 1). Catchment As (5.3 ha) is a sub-catchment of catchment A (49.0 ha). Catchment B (7.0 ha) is adjacent to catchment A. The altitudes range from 439 to 872 m a.s.l. All catchments are steep with slopes of more than 30°. The most common slope direction is east for catchment A and northwest for catchments B and As.

Annual rainfall was 2950 ± 487 mm from 1982 to 2000 (mean and standard deviation; Uchiyama et al., 2014; years with missing data were not included). The annual mean temperature was 12.1 ± 0.4°C (mean and standard deviation) from 2010 to 2014 at the meteorological station (638 m a.s.l.; Figure 1). Large rainfall events occurred mainly during the rainy season from June to July (625 ± 141 mm; mean and standard deviation for 2010–2014), and during the typhoon season from September to October (910 ± 232 mm). Snowfall only occurs once or twice a year from January to March, only accounts for

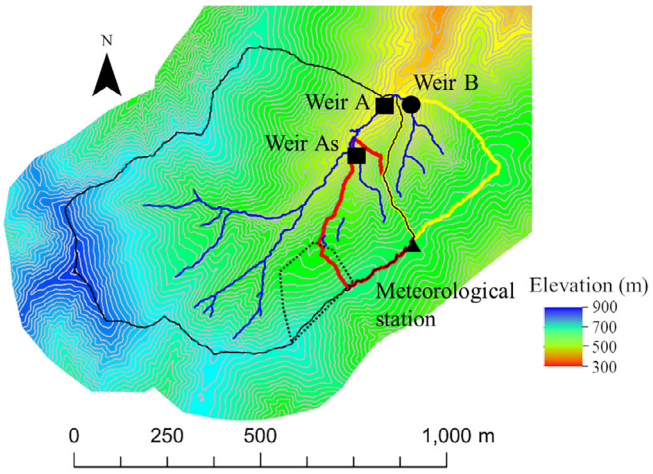

FIGURE 1 Topographic map of the Oborasawa Watershed, where catchment A is denoted by a black line. Catchment As is a subcatchment of catchment A (denoted by a red line), and catchment B is adjacent to catchment A (denoted by a yellow line). Contour interval is 10 m. Blue lines represent surface water. A circle and squares show weirs. A triangle indicates a meteorological station. Rain gauges (tipping-bucket type or plastic bottle type) were located on the side of weirs A and As (squares), and at the meteorological station. A dashed line represents the area which had nondescript watershed boundaries and gentle slopes (see Section 3.3)

a small percentage of total annual precipitation and has limited influence on stream discharge.

The soils in the OEW were classified as Cambisol in accordance with the classification system of the International Union of Soil Sciences Working Group World Reference Base (, 2014). They include a large amount of volcanic ash and have a high infiltration capacity at the surface, ranging from 100 to 600 mm/h (Oda et al., 2013). Average soil depth, observed by a cone penetration test, was 1.64 ± 0.97 m (mean and standard deviation; $n = 217$; Yokoyama et al., 2014). The underlying bedrock beneath the soil is tuff, which is composed mainly of volcanic breccia, and is classified as Cenozoic sedimentary rock (Yokoyama et al., 2014). Based on its chemical characteristics, the bedrock of the western half of catchment A is classified as andesite, basaltic andesite, trachyandesite lava and pyroclastic rocks, whereas that of catchment B, catchment As and the eastern half of catchment A is classified as basalt (based on a geological map of scale 1:200 000 provided by the Geological Survey of Japan, AIST; Figure S1). There is a large fault on the south side of catchment A, which does not pass catchments B and As. Geologic strata are folds, and the anticlinal axis runs north to south or north-northeast to south-southwest. The inclination angle is approximately 60–70° from west to east (Yokoyama et al., 2014). Boring surveys to a depth of 50 m were conducted at two points in and near catchment As. There exists a weathered bedrock with fissures below 40 m depth from the surface at both survey points. Hydraulic conductivities of bedrock depended on the degree of weathering and ranged from 4.7×10^{-5} to 2.6×10^{-6} cm/s ($n = 8$; Yokoyama et al., 2014). At the observation wells installed at these two survey points, the groundwater level fluctuated several meters due to rainfall events, indicating that groundwater recharge and discharge through bedrock occurred in the studied catchments. Thus, we can presume that a shallow and a deep aquifer is formed in the soil layer and the bedrock layer, respectively, and both of them contribute to stream discharge.

Forests cover most of the OEW and the bare land ratio is less than 1%. According to the 2007 vegetation survey, approximately two-thirds of the forested areas are composed of conifers (*Cryptomeria japonica* and *Chamaecyparis obtusa*). The remaining one-third is composed of broadleaf trees (e.g., *Cercidiphyllum japonicum* and *Aesculus turbinate*; Uchiyama et al., 2014). Catchment B was entirely surrounded by deer fences in 2012; however, the effects of deer fences on stream discharge were not observed during the study period.

Oda et al. (2013) examined the annual IGF rate of the three catchments in 2010 using the annual chloride balance method. The input of chloride ions into the catchment, which was obtained by throughfall and stem flow observations and included wet and dry deposition, was 30 kg/ha/year. This value was assumed to be representative of the input of the three catchments. The outputs of chloride ions from catchments A, B and As were 31, 21 and 50 kg/ha/year, respectively. From these results, the annual IGF rate of catchment A was −110 mm/year, which was 5% of the annual stream discharge and considered almost negligible. The annual IGF rate of catchment B was 730 mm/year, indicating that a large amount of groundwater flowed out of the catchment. The annual IGF rate of catchment As was −1580 mm/year, representing a large amount of groundwater flow into the catchment.

2.2 | Observations

We used rainfall (P) and stream discharge (Q) data from 2010 to 2014. The P was continuously measured every 10 min with two 0.5 mm tipping-bucket rain gauges (N78, Nippon Electric Instrument, Tokyo, Japan) located at the meteorological station and on the side of weir A (Figure 1). Each P was corrected by those manually measured with polyethylene plastic bottles at the meteorological station and on the side of weir As, respectively. The corrected P per tip was calculated by dividing the manually observed P by the number of tips at the period. As a result, we obtained two daily rainfalls, P_m and P_w, which were the daily rainfall at the meteorological station and near the weir, respectively. The amount of P at each point did not greatly differ ($P_m = 0.98\ P_w - 0.03$, $R^2 = 0.96$). The average of these two p-values was used in this study.

Stream water level was measured every 10 min by a pressure-type water level gauge (ATM_N type, Koshin Denki, Tokyo, Japan) installed at the weirs for each catchment and Q of the catchments was calculated considering the empirical relationships between water level (H (m)) and Q ($m^3\ s^{-1}$). When the water level does not exceed the height of the V notch (H_V: 0.644 m for weir A and 0.500 m for weirs B and As), the relationship is given by:

$$Q = aH^b \quad (1)$$

where a and b are empirical coefficients ($b = 2.7443$ for all three weirs: $a = 0.9857$ for weir A and $a = 0.5329$ for weirs B and As). When the water level exceeds H_V, the relationship is described as:

$$Q = \frac{2}{3}c\sqrt{2g}B(H - H_V)^{\frac{3}{2}} + aH_V{}^b \quad (2)$$

where B is the width of the channel (= 3.0 m), g is gravitational acceleration (= 9.8 m s^{-2}) and c is an empirical coefficient ($c = 0.4946$ for weir A and $c = 0.2795$ for weirs B and As). We calculated the specific discharge by dividing the volume of Q by the catchment area. Hereafter, stream discharge (Q) refers to specific discharge. Figure S2 shows temporal changes in daily P and Q from 2010 to 2014.

There were some missing periods for Q of the three catchments (-Table S1). When the periods were short (<50 h) and had little P (<5 mm), we estimated Q by linearly connecting Q before and after the missing periods and used the data for all analyses. We omitted the other missing data periods in sub-annual catchment water balance analyses. The length of the omitted periods were 101 days, 20 days and 1 day for catchments A, B and As, respectively (corresponding to 5.53%, 1.10% and 0.05% of total periods for catchments A, B and As, respectively). Note that these omitted periods were used for calculating the annual Q and annual water loss using either linear connections between Q before and after the missing periods or a rainfall-runoff model (HyCy model, Fukushima, 1988; Table S1).

Air temperature and solar radiation were measured at the meteorological station using a relative humidity probe (HT-20, Azbil, Tokyo, Japan) and a pyranometer (SL-30, Azbil, Tokyo, Japan), respectively. The measurements and corrections of the meteorological data are described in detail in Figure S3. All meteorological data were observed every 10 min.

2.3 | Analysis

The catchment water balance in a specific period t_A to t_B is described as (Figure 2):

$$\int_{t_A}^{t_B} P\,dt = \int_{t_A}^{t_B} Q\,dt + \int_{t_A}^{t_B} L\,dt + \Delta S \quad (3)$$

$$\text{in which } \int_{t_A}^{t_B} L\,dt = \int_{t_A}^{t_B} ET\,dt + \int_{t_A}^{t_B} IGF\,dt \quad (4)$$

where t is the time and L is the catchment water loss, which is defined as the sum of ET and IGF. ΔS is the change in catchment water storage between before and after the water balance period. The cumulative L in the specific hydrological period t_A to t_B, that is, the second term on the right side of Equation (3), can be calculated by the STWB (Linsley et al., 1958; see Figure 2).

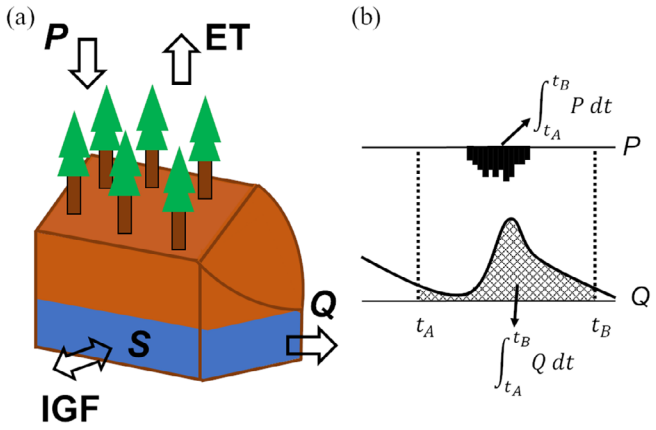

FIGURE 2 Schematic diagram of the short-term water balance method. The period from time A (t_A) to time B (t_B) is one water balance period. Q, P, ET, S and IGF refer to stream discharge, rainfall, evapotranspiration, catchment water storage and inter-catchment groundwater flow, respectively

The STWB assumes that if Q at t_A and t_B, several days after the last rainfall, show similar values, the catchment water storages at t_A and t_B are also similar, resulting in $\Delta S \approx 0$ in Equation (3). This assumption might be close to the assumption that Q can be expressed by a single-valued function of water storage in the catchment, which has been considered a good approximation in many catchments (Kirchner, 2009). There was no standard method for choosing the start and end dates of the hydrological period, that is, t_A and t_B. We used the method proposed by Suzuki (1985), as well as Kosugi and Katsuyama (2007), with a slight change in threshold values. Specifically, we followed the procedure described below to extract various pairs of time points:

1. Determine all days where no rain fell during the previous 2 days as the potential start and end days for water balance periods.
2. Select all pairs from these candidate days, such that the daily Q of the later day is within 5% of the earlier day.
3. Omit pairs of days that encompass more than 85 days.
4. Omit pairs of days that encompass periods with less than 30 mm of P.

For the first criterion, the 2-day threshold was used to exclude the effect of direct runoff immediately after rainfall that might have a large influence on ΔS (Suzuki, 1985). Note that the potential days extracted can be used as the start and end days several times. This meant that the STWB allowed that a certain day is included in several water balance periods and that overlaps in water balance periods occurred. The second criterion was used to extract combinations of days with similar Q values that were expected to result in similar water storage. We selected the 5% threshold because this value is similar to the daily rate of decrease in Q (e.g., the average daily decrease rate was 3.8% for less than 5 mm/day Q of catchment A) and thus suitable for extracting combinations of days with similar

Q values during temporal decreases in Q. For the third criterion, we chose 85 days as the threshold value because it was long enough to obtain a sufficient number (approximately >100) of extracted periods in order to compare IGF values with hydrological factors such as P and Q of the periods. In addition, if we had selected a greater number of days as the threshold value, the water balance periods extracted would have included many rainfall events and probably several dry/wet conditions as well. This might have caused difficulties in comparing IGF values and hydrological factors. The fourth criterion was used because at least one of the water balance components needed to be markedly larger than zero to avoid the effect of ΔS (assuming $\Delta S \approx 0$). The 30 mm threshold was a value similar to the average minimum monthly P, which was 34 mm from 2010 to 2014, and was less likely to produce long (>1 month) non-extracted periods. We described the effects of these threshold values on our results in the Results and Discussion (see Section 3.2).

In this study, using the STWB, Equation (3) with $\Delta S = 0$ (because of similar Q between the certain points in time), we estimated IGF on the premise that ET was given as well as P and Q (see Equations 3 and 4). For simplicity, we assumed that the primary forcing variable for ET is radiative energy in Japanese coniferous plantations (Kumagai et al., 2008). Hence, we used a modified Priestley and Taylor (1972) expression to calculate the daily ET given by:

$$\mathrm{ET} = \alpha \frac{\Delta}{\Delta + \gamma} \cdot \frac{R_n}{\lambda} \tag{5}$$

where α is the Priestley and Taylor coefficient, Δ is the slope of the saturation water vapour pressure (Pa/K), γ is the psychrometer constant (66 Pa/K) and λ is the latent heat of vaporization of water (2.4×10^6 J/kg). R_n is the daily cumulative net radiation (J/m^2/day), which was assumed to be the daily cumulative solar radiation multiplied by 0.8 (Komatsu et al., 2007). ET was calculated on a daily time step, and the input data were the average air temperature for calculating Δ and the daily cumulative solar radiation. In this site, ET was assumed to be limited by solar radiation and occur mainly in daylight hours; therefore, we used the daylight hour average temperature as an input instead of the 24-h average temperature. In this study, the average temperature and the cumulative solar radiation were calculated from 0600 to 1800LT, which was the approximate daylight hours, in order to simplify calculations.

A major uncertainty in Equation (5) is α, which is usually less than the typical value of 1.26, for forest ET because of additional aerodynamic and within-tree resistances (see Kumagai et al., 2004). We used annual water balance-measured ET to obtain the annual mean α and proceeded to calculate daily ET using Equation (5) with α and R_n. The annual mean α was computed as follows: Total water loss of catchment A, where annual IGF rate $\approx$ 0 (Oda et al., 2013), from 2010 to 2014 was derived from the total catchment water balance. Then we assumed that total water loss was equivalent to an integrated daily ET (Equation 5) over the period 2010–2014, determining the annual mean α (0.897) over the period. Note that calculating each year's α from the annual water balances of catchment A from 2010 to 2014 gives $\alpha = 0.900 \pm 0.113$ (mean ± standard deviation; This standard deviation corresponds to approximately 100 mm/year), which was not significantly different from the interannual value of 0.897 (Figure S4). Seasonal patterns of daily ET over the years, calculated using Equation (5) with the determined α, are shown in Figure S2.

As a result, rearranging Equations (3) and (4) gives the IGF in the specific hydrological period as:

$$\int_{t_A}^{t_B} \mathrm{IGF} dt = \int_{t_A}^{t_B} P dt - \int_{t_A}^{t_B} Q dt - \int_{t_A}^{t_B} ET dt \tag{6}$$

The daily IGF rate is obtained by dividing $\int_{t_A}^{t_B} \mathrm{IGF} dt$ by the length of the specific water balance periods in each case ($t_B - t_A$, in this case). Positive IGF means that groundwater flows out of the catchment, and negative values mean that groundwater flows into the catchment. Because we calculated IGF using the water balance of catchments, any groundwater that did not flow into the stream was considered as lost to that particular catchment and estimated as positive IGF. When groundwater that flowed into a targeted catchment flowed out from the catchment without passing through the weir, such groundwater flow was not considered as IGF because the groundwater was not involved in both P and Q of the catchment. In this paper, water storage refers to the total amount of water in a catchment. However, we did not include groundwater in the above two cases as water storage.

We estimated the uncertainty in IGF derived from Equation (6) using standard techniques to calculate the propagation of uncertainty, that is, the square root of the sum of the squared uncertainties (Genereux et al., 2005):

$$W_{\mathrm{IGF}} = \sqrt{\left(\varepsilon_P \int_{t_A}^{t_B} P dt\right)^2 + \left(\varepsilon_Q \int_{t_A}^{t_B} Q dt\right)^2 + \left(\varepsilon_{\mathrm{ET}} \int_{t_A}^{t_B} \mathrm{ET} dt\right)^2} \tag{7}$$

where W_{IGF} (mm) is the uncertainty in the IGF of the targeted water balance period and ε_P, ε_Q and ε_{ET} are the ratios of the uncertainties in the observed values of P, Q and ET, respectively. ε_P was estimated from the P observed at two points (P_1 and P_2) as follows:

$$\varepsilon_P = \overline{\left(\frac{|P_1 - P_2|}{P_1 + P_2}\right)} \tag{8}$$

where the horizontal bar indicates the average of all observations. ε_P was set to 0.025 based on our observations from 2010 to 2014. ε_Q was estimated using the Q calculated from H (Q_{cal}) and the manually observed Q (Q_{obs}) as follows:

$$\varepsilon_Q = \overline{\left(\frac{|Q_{\mathrm{obs}} - Q_{\mathrm{cal}}|}{Q_{\mathrm{cal}}}\right)} \tag{9}$$

ε_Q was set to 0.156 for catchment A, and 0.137 for catchments As and B. $\varepsilon_{\mathrm{ET}}$ was set to 0.126 based on the above-mentioned mean and standard deviation of α (i.e., $\varepsilon_{\mathrm{ET}} = 0.113/0.900$).

3 | RESULTS AND DISCUSSION

3.1 | IGF calculations using the STWB

The IGF rates and their temporal trends were largely different among the three catchments (Figures 3 and 4). The numbers of extracted water balance periods at catchments A, B and As were 303, 311 and 215, respectively. The IGF rates of catchment A varied from −4 to 5 mm/day and were positive from September to December and negative from January to March and from July to August (Figure 3a). The IGF rates of catchment B were positive in most cases and varied from −2 to 6 mm/day (Figure 3b). In particular, IGF showed large positive values from September to October. Conversely, the IGF rates of Catchment As were negative in most cases and varied from −11 to 8 mm/day (Figure 3c). IGF often showed large negative value from September to October and sometimes displayed positive values from January to March. Annual IGF rate, which was calculated by subtracting annual ET from annual water loss, was 0 ± 105, 317 ± 137 and −840 ± 373 (mean ± standard deviation; mm/year) for catchments A, B and As, respectively. Annual IGF of catchment B and As corresponded to 10.4% and 27.7% of annual *P*, respectively. The IGF of three catchments exhibited statistically significant linear relationships with *P* and *Q* (Figure 4). In particular, increases in *P* and *Q* induced a significant increase in IGF outflow from catchment B (Figure 4e,f) and a drastic increase in the inflow to catchment As (Figure 4i,j). Even considering the uncertainties, these trends were obvious (Figures 3 and 4) and did not have seasonal changes (Figure S5).

3.2 | Validity of our IGF calculations

The STWB assumes that at times when *Q* is similar, the water storage is also similar. However, this assumption might not always be valid.

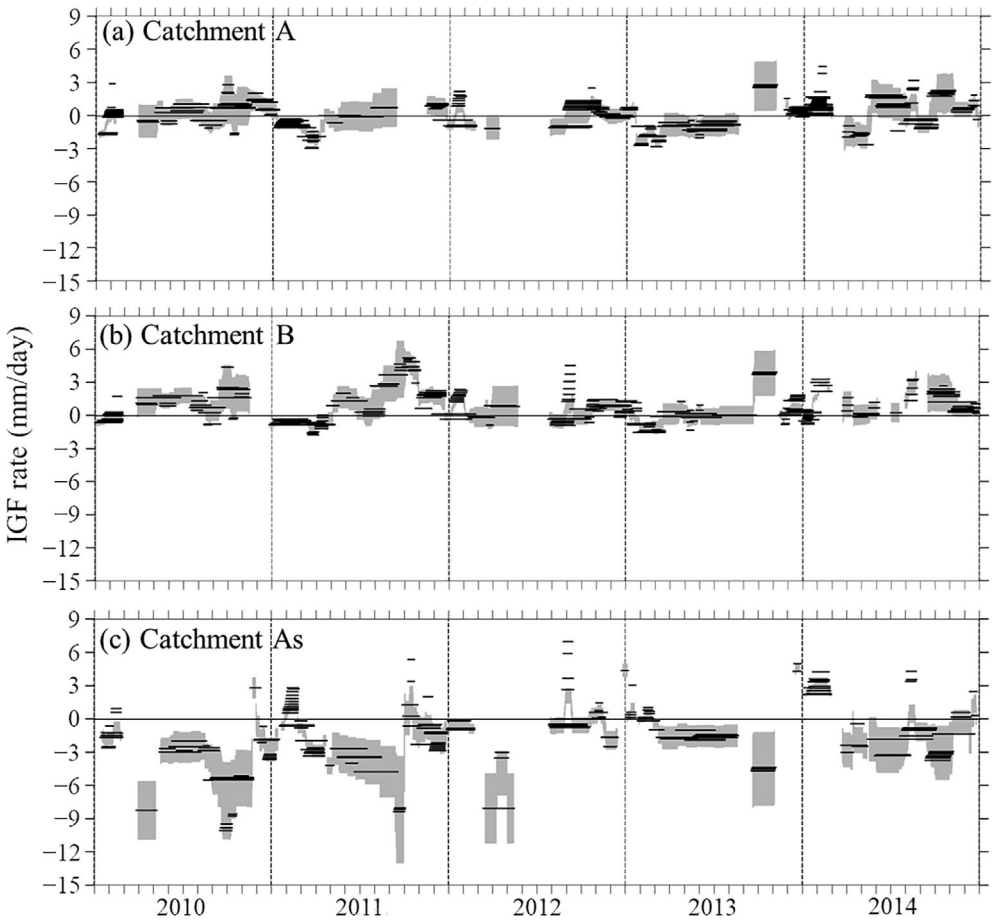

FIGURE 3 Temporal changes in inter-catchment groundwater flow (IGF) rates from 2010 to 2014. Positive values indicate that groundwater flows out of the catchment, and negative values show that groundwater flows into the catchment. Each bar corresponds to a period when the water balance was calculated. The length of each bar indicates the length of each period. The IGF value shown by each bar is the daily IGF rate calculated by dividing the IGF in Equation (6) by the length of periods. The grey shaded area is the range of the uncertainty of the daily IGF rate calculated as below. First, we calculated the daily uncertainty for each water balance period by dividing the IGF uncertainty of a water balance period in Equation (7) by the length of the period. Then, we obtained average values for each day in which the calculated IGF value existed. Specifically, when a certain day was included in several water balance periods, we calculated the average of the daily IGF rate and its uncertainty from all water balance periods that included the day and showed their range with the grey area

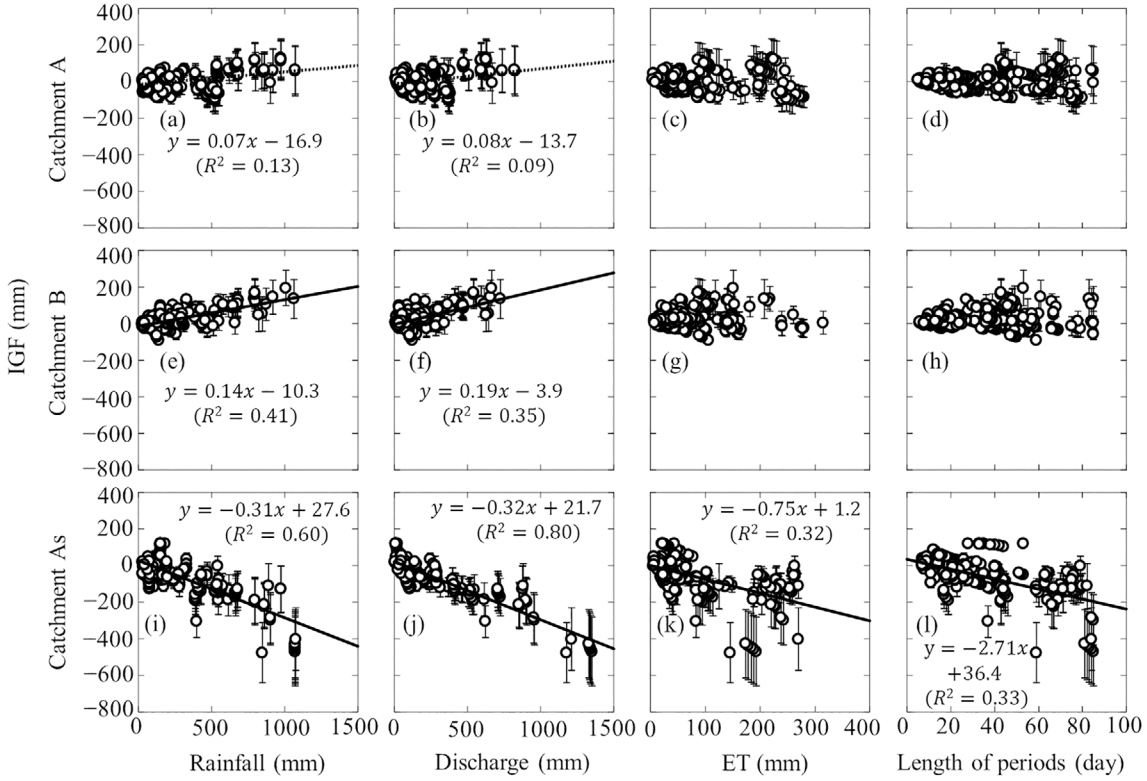

FIGURE 4 Relationships between the inter-catchment groundwater flow (IGF) and hydrological factors. One point corresponds to a period when the water balance was calculated. The linear regression lines were drawn when *p*-values of the slopes of the regression lines were less than 0.01. The solid and the dotted lines were used for the regression lines with more and less than 0.3 of the *R*-squared value, respectively. The error bars indicate the IGF uncertainty calculated by the uncertainty analysis

Several recent studies focused on and re-recognized that the water dynamics in surface soil are sometimes decoupled from those of *Q* (Brooks et al., 2010; Tashie et al., 2019). In addition, temporal variations in groundwater levels in bedrock often differ greatly from those of *Q* (Gabrielli et al., 2012; Kosugi et al., 2011) That is, even when *Q* is similar, the water storage is not always similar; ΔS cannot be assumed to be zero and would affect the estimated IGF values. In addition, the threshold values used in our calculations (see Section 2.3) might have influenced ΔS.

Therefore, we first recalculated the IGF of the three catchments by changing the threshold values of the STWB (as in Section 2.3) from 85 to 120 days (Figure S6a), 30 to 15 mm of rainfall (Figure S6b), and 5% to 3% of the difference in *Q* (Figure S6c). The differences between the results of these calculations (Figure S6) and those of the original (Figure 4) were small. For example, the maximum changes in the slopes of regression lines plotted for catchment B were from 0.14 to 0.17 for *P* and 0.19 to 0.26 for *Q* (Figure 4 and Figure S6a). In catchment As, there was only a 0.01 change in the slopes of regression lines against *P* and *Q* (Figures 4 and Figure S6). Therefore, the differences in the threshold values of the STWB did not affect the interpretation of our results.

Second, we examined the effects of ΔS using soil moisture and groundwater level data obtained from the OEW (Figure S7). There were high ΔS values in each water balance period; the changes in soil moisture and groundwater storage ranged from −32 to 20 mm and −113 to 125 mm, respectively. However, the average changes in soil moisture and groundwater storage were only −1.5 and −6.8 mm, respectively. In addition, there were no seasonal trends in the changes of subsurface storage (Figure S7b,c). Although there were weak positive correlations between the change in groundwater storage and *P* or *Q*, their moving averages showed that the values of the changes were low (< 15 mm) when the *P* and *Q* values were high (>400 mm; Figure S7e,g). That is, the effects of ΔS on the IGF were large for each water balance period. However, when the average IGF behaviour with multiple water balance periods was examined, the effects of ΔS decreased compared to a single water balance period. For example, we used many water balance periods to obtain the regression lines in Figure 4; therefore, the effects of ΔS on the regression lines are likely to be negligible.

Third, we assessed the influence of redundancy on IGF calculations because the STWB allowed for a certain day to be included in multiple water balance periods and for overlaps in water balance periods to occur (see Section 2.3; Figure S8). Specifically, for a certain water balance period, we extracted water balance periods that shared 60% or more days with each other and calculated the average IGF, *P*, *Q*, ET and the length of periods. These operations were performed in ascending order of the start date of the water balance periods; once used, water balance periods were excluded from subsequent

operations. Results showed that the number of water balance periods in catchments A, B and As were 87, 102 and 70, respectively. Overall trends did not change from Figure 4, and the slopes and intercepts of the regression lines were almost the same as those in Figure 4 (Figure 4 and Figure S8).

Finally, we confirmed the impact of the spatiotemporal uncertainty of ET on the calculations of IGF. Potential ET is generally likely to be influenced by the slope aspect because of the difference in received solar radiation (Stephenson, 1998). Catchments B and As are northwest-facing, and might experience less ET than catchment A (Figure 1). At a conifer plot in catchment As, the interception ratio was 0.14, which was approximately 400 mm/year, and the transpiration rate was 593 mm/year (Fujime et al., 2021). The sum of these values is 993 mm/year, which is 18.6% higher than the five-year average annual loss of catchment A. This value is only slightly higher than the value of 12.6% considered in the uncertainty analysis. When 18.6% was used in the uncertainty analysis instead of 12.6%, the increase in uncertainty in IGF for each water balance period was 2.3 ± 2.6 (mean ± standard deviation; mm). That is, the spatial uncertainty of ET in our catchments did not have a significant influence on the IGF calculations.

3.3 | Estimations of IGF driving processes in OEW

Catchments B and As have similar slope directions, catchment areas, soil types and bedrock type and are not affected by a large fault (Figure 1 and Figure S1). Nevertheless, there was a large difference in their IGF characteristics (Figures 3 and 4). The differences between the two catchments might be explained by two potential IGF mechanisms: infiltration and subsequent discharge through the bedrock (Graham et al., 2010; Kormos et al., 2015), and the difference in area between the surface catchment boundary (defined by surface topography) and the actual hydrological boundary (which is influenced by subsurface structure; hereinafter referred to as A_{dif}; Hess et al., 1989; Jukić & Denić-Jukić, 2009). In our catchments, a weathered bedrock with fissures existed at a depth of 40 m from the surface at two boring survey points in and near catchment As. Geologic strata slope from the west to east at an angle of 60°–70° (Yokoyama et al., 2014), which was steeper than the topographic slope. If groundwater flows along the slope of the bedrock, it is expected to infiltrate deep inside the catchment and discharge outside the catchment, resulting in positive IGF values. We, therefore, presume that infiltration through the bedrock would be the main reason for positive IGF values for catchment B, while the difference in area between the surface catchment boundary and the actual hydrological boundary would be the main reason for negative IGF values for catchment As.

Our methods would be useful to consider this presumption, and the results shown in Figure 4 and the topographic map support it. If the discrepancy in area between the surface catchment boundary and the actual hydrological boundary occurred, the slope between the IGF and P (k_P), which was 0.14 and −0.31 for catchments B and As, respectively (Figure 4e,i), can be roughly related to A_{dif}. In our catchments, approximately 70% of the P contributed to Q (cf. Table S2; the ET rate of catchment A, in which IGF could be negligible, was 30% of rainfall). Neglecting the intercept of the linear function, IGF can be expressed as:

$$\mathrm{IGF} = \frac{0.7 \times P \times A_{\mathrm{dif}}}{A_C} = k_P \times P \tag{10}$$

Rearranging to obtain A_{dif},

$$A_{\mathrm{dif}} = \frac{k_P \times A_C}{0.7} \tag{11}$$

where A_C is the catchment area. In this study, A_C was calculated based on 1 − m DEM under the assumption that all water flowed in the direction of steepest descent. This equation gave 1.6 and 2.4 ha as A_{dif} for catchments B and As, respectively. If there exist areas that contain nondescript watershed boundaries, these values of A_{dif} would account for IGF. The actual hydrological boundary influenced by the bedrock topography can be significantly different from the surface boundary (Freer et al., 2002) especially within the area of nondescript watershed boundaries. In catchment B, the ridge terrain was clear (Figure 1), and A_{dif} was unlikely to occur. Conversely, the west side of catchment As had nondescript watershed boundaries and gentle slopes, that is, the area surrounded by a dashed line in Figure 1. This area had no surface water, and its size was approximately 2.5–3 ha and was almost equivalent to the above estimation. Therefore, for catchment As, the difference between the surface catchment boundary and the actual hydrological boundary was a plausible reason for the negative IGF. In contrast, infiltration into the bedrock might explain the mechanism that formed the positive IGF of catchment B. In addition, the area with the nondescript watershed boundary of catchment As is located within catchment A and not included in catchment B (Figure 1). Therefore, the above hypothesis was consistent with the result that the annual water balance was almost closed in catchment A, although it contained catchment As. Besides, when we applied the same method for catchment A, the A_{dif} was 4.9 ha. We could not find nondescript watershed boundaries around catchment A that caused such large discrepancies in catchment area (Figure 1). Therefore, the difference between the catchment boundary defined by the surface topography and the actual hydrological boundary was not likely to occur for catchment A.

The intercepts in the IGF function of P or Q might contain additional information (Figure 4). In particular, the IGF in catchment As had statistically significant positive intercepts in both the relationships with P and Q. This suggests that groundwater outflow from catchment As occurred even when there was minimal P and Q. Further, it should be noted that while groundwater flowed into catchment As from an adjacent catchment, it always flowed out of this catchment. Because of this, only catchment As might have undergone water depletion in 2013 and 2014 (Figure S1), resulting in a large interannual variation in Q in catchment As (Table S2). As mentioned above, groundwater could easily infiltrate the bedrock in our catchments.

Thus, groundwater infiltration through bedrock and discharge outside catchments might also occur in catchment As, and its effects might only be observed in dry periods. In addition, a previous study reported that the direction of water flow between streams and groundwater changed seasonally due to fluctuations in groundwater level (Zimmer & McGlynn, 2017), and this phenomenon could occur in catchment As. Therefore, one of the future tasks to verify these possibilities is to observe the temporal variation of groundwater level in and near catchment As.

Compared to the other catchments, catchment A has a one order larger catchment area and a larger difference in elevation within the catchment. Moreover, there is spatial heterogeneity in the bedrock characteristics of catchment A (Figure S1). There are two possible reasons for the near negligible IGF of catchment A, unlike the other two catchments: the difference in bedrock caused a difference in permeability such that less groundwater of catchment A infiltrated into bedrock than catchments B and As, or groundwater that infiltrated into bedrock discharged to the surface soil and streams as the altitude decreased. These possibilities can be verified in the future by examining where and how much groundwater is discharged to streams with multipoint observations of stream discharge and water chemistry (Egusa et al., 2016).

3.4 | Applicability of our methods

This study presents an IGF estimation method using the STWB. The method assumed that when the difference in stream discharges between certain points in time is small, the difference in water storage between those points in time is also small. As shown in Section 3.2, this assumption was not always valid for individual water balance periods in the STWB. However, it would still be valid when determining the relationships between IGF and hydrological factors by using many water balance periods. Kirchner (2009) assumed that Q could be expressed using a single-valued function of water storage in a catchment and suggested a simple rainfall-runoff model. Our assumption is close to this assumption, which has been considered a good approximation in many catchments (Kirchner, 2009). Actually, many subsequent studies have used Kirchner's model and showed the model could reproduce Q well (Hailegeorgis et al., 2016; Melsen et al., 2014; Teuling et al., 2010). Therefore, the assumption in Kirchner (2009) and similar STWB assumptions can be valid in many catchments, implying the high potential applicability of our method.

The proposed method complements existing methods and further advances IGF research. It can be used to calculate IGF for a finer time scale than possible using the annual water and mass balances. Furthermore, this method requires less data than the estimation method based on Darcy's law and multiple points of groundwater level data. Compared to the method using rainfall-runoff models, our method does not require model structures to be determined or parameter fitting to be performed; therefore, the equi-finality problem is less likely to be an issue. In addition, our method can also be used to diagnose and select IGF model structures for inclusion in rainfall-runoff models. For example, although this study indicated in a simple way using the relationship between IGF and the sum of Q (Figure 4b,f,j), any function of Q such as $cQ^d + e$ (c, d and e are constants) can be used and the optimum parameters c, d and e obtained; this reproduces the IGF obtained by the STWB. The IGF expressed by the function of Q can be converted into a function of water storage according to the structure of rainfall-runoff models. This is less computationally intensive than parameter fitting of rainfall-runoff models with IGF sub-models and is not affected by other model parameters. Therefore, our method could be particularly useful for formulating complex phenomena, such as those observed in catchment As in this study, without prior information. The strength of our method is that sub-annual IGF can be calculated easily from P and Q data if adequate ET values can be obtained. Although this study used the Priestley and Taylor equation to calculate ET, other methods such as sap flux and eddy covariance can be also used to obtain ET. Therefore, calculating sub-annual IGF and elucidating its driving factors using our methods could be a promising approach for modelling IGF in catchments with a wide range of geological and climatological conditions.

ACKNOWLEDGEMENTS

This study is a part of the project focusing on the conservation of the natural environment through the assessment of forest hydrological function, sponsored and supported by the Kanagawa Prefectural Government, Japan. We thank the staff of Kanagawa Prefecture Natural Environment Conservation Centre for managing the experimental watershed and data collection. We also thank Takahide Yokoyama for insight into site bedrock geology, and lab members for their technical assistance.

DATA AVAILABILITY STATEMENT

The data that support the findings of this study are available from the corresponding author, upon reasonable request.

ORCID

Tomohiro Egusa https://orcid.org/0000-0001-8993-1044
Tomoki Oda https://orcid.org/0000-0003-1677-4425
Takanori Sato https://orcid.org/0000-0003-1483-966X
Tomo'omi Kumagai https://orcid.org/0000-0001-8331-271X

REFERENCES

Aishlin, P., & McNamara, J. P. (2011). Bedrock infiltration and mountain block recharge accounting using chloride mass balance. *Hydrological Processes*, *25*(12), 1934–1948. https://doi.org/10.1002/hyp.7950

Beven, K. (1993). Prophecy, reality and uncertainty in distributed hydrological modelling. *Advances in Water Resources*, *16*(1), 41–51. https://doi.org/10.1016/0309-1708(93)90028-E

Bouaziz, L., Weerts, A., Schellekens, J., Sprokkereef, E., Stam, J., Savenije, H., & Hrachowitz, M. (2018). Redressing the balance: Quantifying net intercatchment groundwater flows. *Hydrology and Earth System Sciences*, *22*(12), 6415–6434. https://doi.org/10.5194/hess-22-6415-2018

Brooks, J. R., Barnard, H. R., Coulombe, R., & McDonnell, J. J. (2010). Ecohydrologic separation of water between trees and streams in a Mediterranean climate. *Nature Geoscience*, *3*(2), 100–104. https://doi.org/10.1038/ngeo722

Clark, M. P., Slater, A. G., Rupp, D. E., Woods, R. A., Vrugt, J. A., Gupta, H. V., Wagener, T., & Hay, L. E. (2008). Framework for understanding structural errors (FUSE): A modular framework to diagnose differences between hydrological models. *Water Resources Research*, *44*(12), 1–14. https://doi.org/10.1029/2007WR006735

Eakin, T. E. (1966). A regional interbasin groundwater system in the White River Area, southeastern Nevada. *Water Resources Research*, *2*(2), 251–271. https://doi.org/10.1029/WR002i002p00251

Egusa, T., Ohte, N., Oda, T., & Suzuki, M. (2016). Quantifying aggregation and change in runoff source in accordance with catchment area increase in a forested headwater catchment. *Hydrological Processes*, *30*(22), 4125–4138. https://doi.org/10.1002/hyp.10916

Fenicia, F., McDonnell, J. J., & Savenije, H. H. G. (2008). Learning from model improvement: On the contribution of complementary data to process understanding. *Water Resources Research*, *44*(6), 1–13. https://doi.org/10.1029/2007WR006386

Flerchinger, G. N., & Cooley, K. R. (2000). A ten-year water balance of a mountainous semi-arid watershed. *Journal of Hydrology*, *237*(1–2), 86–99. https://doi.org/10.1016/S0022-1694(00)00299-7

Freer, J., McDonnell, J. J., Beven, K. J., Peters, N. E., Burns, D. A., Hooper, R. P., Aulenbach, B., & Kendall, C. (2002). The role of bedrock topography on subsurface storm flow. *Water Resources Research*, *38*(12), 1–16. https://doi.org/10.1029/2001WR000872

Frisbee, M. D., Phillips, F. M., Campbell, A. R., Liu, F., & Sanchez, S. A. (2011). Streamflow generation in a large, alpine watershed in the southern Rocky Mountains of Colorado: Is streamflow generation simply the aggregation of hillslope runoff responses? *Water Resources Research*, *47*(6), 1–18. https://doi.org/10.1029/2010WR009391

Frisbee, M. D., Tysor, E. H., Stewart-Maddox, N. S., Tsinnajinnie, L. M., Wilson, J. L., Granger, D. E., & Newman, B. D. (2016). Is there a geomorphic expression of interbasin groundwater flow in watersheds? Interactions between interbasin groundwater flow, springs, streams, and geomorphology. *Geophysical Research Letters*, *43*(3), 1158–1165. https://doi.org/10.1002/2015GL067082

Fujime, N., Kumagai, T., Egusa, T., Momiyama, H., & Uchiyama, Y. (2021). Importance of calibration in determining forest stand transpiration using the thermal dissipation method. *Agricultural and Forest Meteorology*, 301–302. https://doi.org/10.1016/j.agrformet.2021.108356

Fukushima, Y. (1988). A model of river flow forecasting for a small forested mountain catchment. *Hydrological Processes*. *2*(2), 167–185. https://doi.org/10.1002/hyp.3360020207

Gabrielli, C. P., McDonnell, J. J., & Jarvis, W. T. (2012). The role of bedrock groundwater in rainfall-runoff response at hillslope and catchment scales. *Journal of Hydrology*, *450–451*, 117–133. https://doi.org/10.1016/j.jhydrol.2012.05.023

Genereux, D. P., Jordan, M. T., & Carbonell, D. (2005). A paired-watershed budget study to quantify interbasin groundwater flow in a lowland rain forest, Costa Rica. *Water Resources Research*, *41*(4), 1–17. https://doi.org/10.1029/2004WR003635

Genereux, D. P., Webb, M., & Solomon, D. K. (2009). Chemical and isotopic signature of old groundwater and magmatic solutes in a Costa Rican rain forest: Evidence from carbon, helium, and chlorine. *Water Resources Research*, *45*(8), 1–14. https://doi.org/10.1029/2008WR007630

Graham, C. B., van Verseveld, W., Barnard, H. R., & McDonnell, J. J. (2010). Estimating the deep seepage component of the hillslope and catchment water balance within a measurement uncertainty framework. *Hydrological Processes*, *24*(25), 3631–3647. https://doi.org/10.1002/hyp.7788

Hailegeorgis, T. T., Alfredsen, K., Abdella, Y. S., & Kolberg, S. (2016). Evaluation of storage–discharge relationships and recession analysis-based distributed hourly runoff simulation in large-scale, mountainous and snow-influenced catchment. *Hydrological Sciences Journal*, *61*(16), 2872–2886. https://doi.org/10.1080/02626667.2016.1170939

Hess, J. W., Wells, S. G., Quinlan, J. F., & White, W. B. (1989). Hydrogeology of the south-Central Kentucky Karst. In W. B. White & E. L. White (Eds.), *Karst hydrology concepts from the mammoth cave area* (pp. 15–63). Van Nostrand Reinhold.

IUSS Working Group WRB. (2014). World reference base for soil resources 2014. International soil classification system for naming soils and creating legends for soil maps. World soil resources reports No. 106. FAO, Rome.

Jukić, D., & Denić-Jukić, V. (2009). Groundwater balance estimation in karst by using a conceptual rainfall-runoff model. *Journal of Hydrology*, *373*(3–4), 302–315. https://doi.org/10.1016/j.jhydrol.2009.04.035

Katsuyama, M., Tani, M., & Nishimoto, S. (2010). Connection between streamwater mean residence time and bedrock groundwater recharge/discharge dynamics in weathered granite catchments. *Hydrological Processes*, *24*(16), 2287–2299. https://doi.org/10.1002/hyp.7741

Kirchner, J. W. (2009). Catchments as simple dynamical systems: Catchment characterization, rainfall-runoff modeling, and doing hydrology backward. *Water Resources Research*, *45*(2), 1–34. https://doi.org/10.1029/2008WR006912

Komatsu, H., Hashimoto, S., Kume, T., Yoshifuji, N., Hotta, N., & Suzuki, M. (2007). Seasonal trends in the solar radiation/net radiation ratio above a *Cryptomeria japonica* plantation forest. *Bulletin of Tokyo University Forest*, *117*, 11–19.

Kondo, J., Watanabe, T., & Nakazono, M. (1992). Heat budget evaluation of forest evapotranspiration in Japan. *Tenki*, *39*(11), 685–695.

Kormos, P. R., McNamara, J. P., Seyfried, M. S., Marshall, H. P., Marks, D., & Flores, A. N. (2015). Bedrock infiltration estimates from a catchment water storage-based modeling approach in the rain snow transition zone. *Journal of Hydrology*, *525*, 231–248. https://doi.org/10.1016/j.jhydrol.2015.03.032

Kosugi, K., Fujimoto, M., Katsura, S., Kato, H., Sando, Y., & Mizuyama, T. (2011). Localized bedrock aquifer distribution explains discharge from a headwater catchment. *Water Resources Research*, *47*(7), 1–16. https://doi.org/10.1029/2010WR009884

Kosugi, K., Katsura, S., Katsuyama, M., & Mizuyama, T. (2006). Water flow processes in weathered granitic bedrock and their effects on runoff generation in a small headwater catchment. *Water Resources Research*, *42*(2), 1–18. https://doi.org/10.1029/2005WR004275

Kosugi, Y., & Katsuyama, M. (2007). Evapotranspiration over a Japanese cypress forest. II. Comparison of the eddy covariance and water budget methods. *Journal of Hydrology*, *334*(3–4), 305–311. https://doi.org/10.1016/j.jhydrol.2006.05.025

Kumagai, T., Katul, G. G., Saitoh, T. M., Sato, Y., Manfroi, O. J., Morooka, T., Ichie, T., Kuraji, K., Suzuki, M., & Porporato, A. (2004). Water cycling in a Bornean tropical rain forest under current and projected precipitation scenarios. *Water Resources Research*, *40*(1), 1–12. https://doi.org/10.1029/2003WR002226

Kumagai, T., Tateishi, M., Shimizu, T., & Otsuki, K. (2008). Transpiration and canopy conductance at two slope positions in a Japanese cedar forest watershed. *Agricultural and Forest Meteorology*, *148*(10), 1444–1455. https://doi.org/10.1016/j.agrformet.2008.04.010

Le Moine, N., Andréassian, V., Perrin, C., & Michel, C. (2007). How can rainfall-runoff models handle intercatchment groundwater flows? Theoretical study based on 1040 French catchments. *Water Resources Research*, *43*(6), 1–11. https://doi.org/10.1029/2006WR005608

Linsley, P. K., Kohler, M. A., & Paulus, J. L. H. (1958). *Hydrology for engineers* (pp. 113–116). McGraw-Hill.

Manna, F., Cherry, J. A., McWhorter, D. B., & Parker, B. L. (2016). Groundwater recharge assessment in an upland sandstone aquifer of southern California. *Journal of Hydrology*, *541*, 787–799. https://doi.org/10.1016/j.jhydrol.2016.07.039

Manna, F., Murray, S., Abbey, D., Martin, P., Cherry, J., & Parker, B. (2019). Spatial and temporal variability of groundwater recharge in a

sandstone aquifer in a semiarid region. *Hydrology and Earth System Sciences*, *23*(4), 2187–2205. https://doi.org/10.5194/hess-23-2187-2019

Manning, A. H., & Solomon, D. K. (2005). An integrated environmental tracer approach to characterizing groundwater circulation in a mountain block. *Water Resources Research*, *41*(12), 1–18. https://doi.org/10.1029/2005WR004178

McMillan, H. K., Clark, M. P., Bowden, W. B., Duncan, M., & Woods, R. A. (2011). Hydrological field data from a modeller's perspective: Part 1. Diagnostic tests for model structure. *Hydrological Processes*, *25*(4), 511–522. https://doi.org/10.1002/hyp.7841

Melsen, L. A., Teuling, A. J., van Berkum, S. W., Torfs, P. J. J. F., & Uijlenhoet, R. (2014). Catchments as simple dynamical systems: A case study on methods and data requirements for parameter identification. *Water Resources Research*, *50*, 5577–5596. https://doi.org/10.1002/2013WR014720

Oda, T., Suzuki, M., Egusa, T., & Uchiyama, Y. (2013). Effect of bedrock flow on catchment rainfall-runoff characteristics and the water balance in forested catchments in Tanzawa Mountains, Japan. *Hydrological Processes*, *27*(26), 3864–3872. https://doi.org/10.1002/hyp.9497

Peralta-Tapia, A., Sponseller, R. A., Ågren, A., Tetzlaff, D., Soulsby, C., & Laudon, H. (2015). Scale-dependent groundwater contributions influence patterns of winter baseflow stream chemistry in boreal catchments. *Journal of Geophysical Research: Biogeosciences*, *120*(5), 847–858. https://doi.org/10.1002/2014JG002878

Priestley, C. H. B., & Taylor, R. J. (1972). On the assessment of surface heat flux and evaporation using large-scale parameters. *Monthly Weather Review*, *100*(2), 81–92. https://doi.org/10.1175/1520-0493(1972)100<0081:OTAOSH>2.3.CO;2

Schaller, M. F., & Fan, Y. (2009). River basins as groundwater exporters and importers: Implications for water cycle and climate modeling. *Journal of Geophysical Research*, *114*(D4), D04103. https://doi.org/10.1029/2008JD010636

Stephenson, N. L. (1998). Actual evapotranspiration and deficit: Biologically meaningful correlates of vegetation distribution across spatial scales. *Journal of Biogeography*, *25*, 855–870. https://doi.org/10.1046/J.1365-2699.1998.00233.X

Suzuki, M. (1985). Evapotranspiration estimates of forested watersheds in Japan using the short-time period water-budget method. *Journal of the Japanese Forest Society*, *67*(4), 115–125.

Tashie, A., Scaife, C. I., & Band, L. E. (2019). Transpiration and subsurface controls of streamflow recession characteristics. *Hydrological Processes*, *33*(19), 2561–2575. https://doi.org/10.1002/hyp.13530

Teuling, A. J., Lehner, I., Kirchner, J. W., & Seneviratne, S. I. (2010). Catchments as simple dynamical systems: Experience from a Swiss prealpine catchment. *Water Resources Research*, *46*, W10502. https://doi.org/10.1029/2009WR008777

Thoma, M. J., McNamara, J. P., Gribb, M. M., & Benner, S. G. (2011). Seasonal recharge components in an urban/agricultural mountain front aquifer system using noble gas thermometry. *Journal of Hydrology*, *409*(1–2), 118–127. https://doi.org/10.1016/j.jhydrol.2011.08.003

Thyne, G. D., Gillespie, J. M., & Ostdick, J. R. (1999). Evidence for interbasin flow through bedrock in the southeastern Sierra Nevada. *Geological Society of America Bulletin*, *111*(11), 1600. https://doi.org/10.1130/0016-7606(1999)111<1600:EFIFTB>2.3.CO;2

Uchiyama, Y., Nakajima, N., Yokoyama, T., & Yamanaka, Y. (2014). Report on hydrological observations by forest conservation project in Ohbora-sawa Watershed in the Tanzawa Mountains. *Results of Scientific Research on the Tanzawa Mountains*, *12*, 17–26.

Voeckler, H. M., Allen, D. M., & Alila, Y. (2014). Modeling coupled surface water—Groundwater processes in a small mountainous headwater catchment. *Journal of Hydrology*, *517*, 1089–1106. https://doi.org/10.1016/j.jhydrol.2014.06.015

Wang, D. (2011). On the base flow recession at the Panola Mountain research watershed, Georgia, United States. *Water Resources Research*, *47*(3), 1–10. https://doi.org/10.1029/2010WR009910

Yokoyama, T., Uchiyama, Y., & Mitsuhashi, M. (2014). Study on hydrogeological features of Ohbora-sawa watershed in the eastern Tanzawa Mountains. *Results of Scientific Research on the Tanzawa Mountains*, *12*, 1–16.

Zanon, C., Genereux, D. P., & Oberbauer, S. F. (2014). Use of a watershed hydrologic model to estimate interbasin groundwater flow in a Costa Rican rainforest. *Hydrological Processes*, *28*(10), 3670–3680. https://doi.org/10.1002/hyp.9917

Zimmer, M. A., & McGlynn, B. L. (2017). Bidirectional stream-groundwater flow in response to ephemeral and intermittent streamflow and groundwater seasonality. *Hydrological Processes*, *31*(22), 3871–3880. https://doi.org/10.1002/hyp.11301

SUPPORTING INFORMATION

Additional supporting information may be found in the online version of the article at the publisher's website.

How to cite this article: Egusa, T., Oda, T., Sato, T., & Kumagai, T. (2021). Estimation of sub-annual inter-catchment groundwater flow using short-term water balance method. *Hydrological Processes*, *35*(9), e14368. https://doi.org/10.1002/hyp.14368